Performance analysis of PERC bifacial silicon solar cells by combining radiative cooling and light trapping strategies based on surface texturing

1. COMPLEX REFRACTIVE INDEX VALUES EMPLOYED IN NUMERICAL CALCULATION

1.1. 0.3-5 μm RANGE (VISIBLE and NEAR INFRARED)

Fig. S1 shows a cross-section schematic of the flat PERC solar panel designed. Each face is composed of a glass encapsulation layer and an Anti-Reflective-Coating layer. The silicon layer has three regions with different doping. The simulations of the BSC were carried out from the complex refractive index data of the former materials, which were derived from the scientific literature. The complex refractive index of soda-lime-low-iron glass is taken from Rubin [1]. The refractive index of crystalline silicon was fitted: from 0.3 to 1.45 μm was taken from [2], between 1.45 and 3 μm was taken from [3], whereas beyond 3 μm was taken from [4] data. We fitted the data to avoid discontinuities in the boundary between them. The extinction coefficient of doped silicon was modeled considering experimental data and three parametric models. Following the results presented by [7], we employed the data from Green et al. for the wavelengths below the bandgap (λ<1.15). The model published by Vardanyan et al. [8] was used to calculate the extinction coefficient of the doped layers from 1.15 μm to 6 μm. Finally, the divergences between the model of Vardanyan and Green's data in the emitter layer forced us to use the model proposed by Baker-Finch et al. [9] near the bandgap (0.85-1.5 um). The obtained extinction coefficient for the three doped layers was compared to previous publications [5,6] with good agreement in all cases. Regarding the ARC coating, we have considered the silicon nitride (Si_3N_4) and its data was taken from [7] and [8] in the range of 0.3-5 μm. A graphical summary of the employed data is presented in Fig. S2 and S3, respectively.

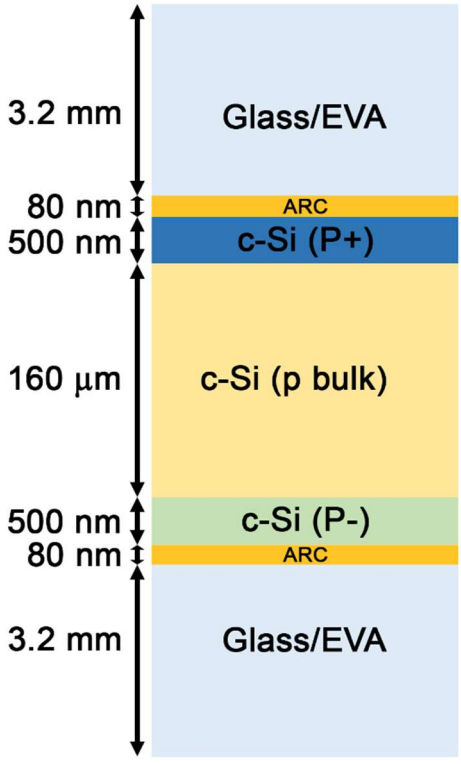

Fig. S1. Cross section schematic of the modelled encapsulated PERC Bifacial solar cell.

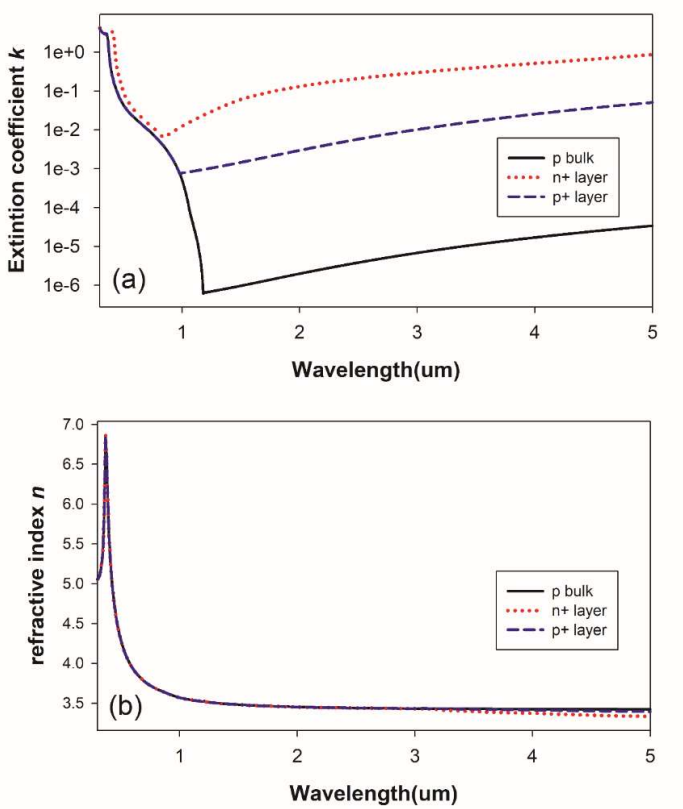

Fig. S2. Refractive index (a) and extinction coefficient (b) of silicon used in the model of PERC bifacial solar cell: p bulk (solid black line), n+ (doted red line) and p+ (blue dashed line).

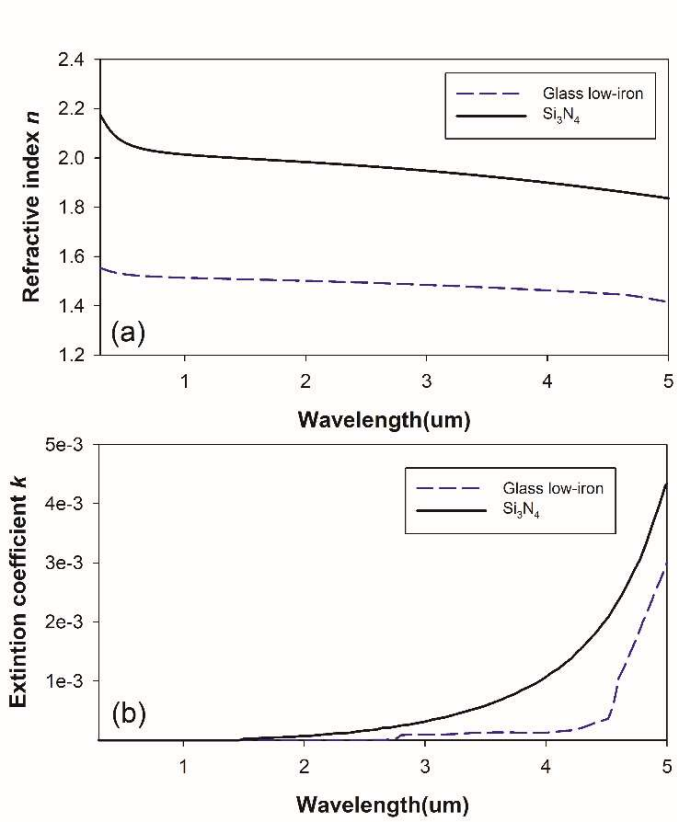

Fig. S3. Refractive index (a) and extinction coefficient (b) of glass low-iron (solid black line) and silicon nitride Si_3N_4 *(Dashed blue line) used in the model of PERC bifacial solar cell.*

Typically, bifacial silicon solar cells are encapsulated employing ethylene vinyl acetate (EVA) and then covered with a soda-lime-low-iron glass on both sides. EVA presents a refractive index almost identical to soda-lime-low-iron glass in the optical and IR ranges, and it allows modeling of both layers together for absorptivity/emissivity calculations. Ideally, the light does not reflect in the interface glass-EVA, and the optical coupling is perfectly matched. Both materials only diverge in the ultraviolet region, where the EVA presents a higher absorption than glass, but these differences do not affect the calculations. From here on, the encapsulation layer of the bifacial PERC solar cell will be modeled as a homogenous 3.2 μm thickness layer of soda-lime-low-iron glass [5].

1.2. 5-25 μm RANGE (MID INFRARED)

In the MIR region (λ>5 μm), soda-lime glass absorbs all the incident IR radiation with no transmission to lower layers achieving an average absorptivity close to 0.87 from 5 to 25 μm. In terms of simulation design, the model of a bifacial solar cell can simplify by assuming that the light does not go through the encapsulation layer in the MIR region. Thus, the simulations of absorptivity/emissivity between 0.3 and 5 μm employ the complete model of the solar cell, whereas the simulations from 5 μm take only into account the encapsulation layer of glass. The complex refractive index and extinction coefficient of the encapsulation employed in this range are shown in Fig. S4.

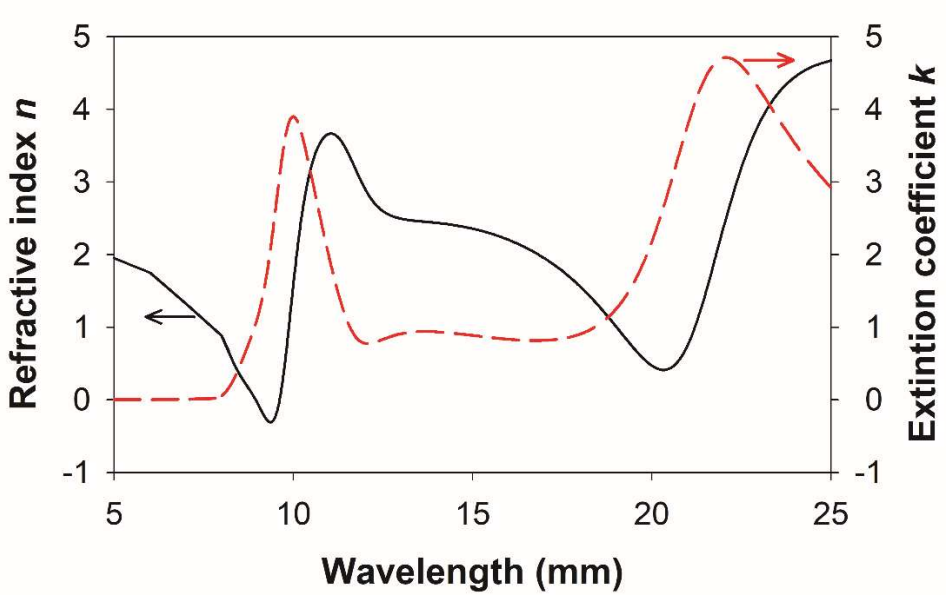

Fig. S4. Refractive index (black solid line) and extinction coefficient (red dashed line) of glass low-iron used in the model of PERC bifacial solar cell from 8 to 25.

2. EVALUATION OF RADIATIVE POWER BALANCE OF THE BIFACIAL SOLAR CELL

2.1. EVALUATION OF ABSORBED PHOTOCURRENT

In the GD-Calc simulation and considering the generated photocurrent, the only useful absorption is the one that occurs in the doped crystalline silicon layers since the other layers are parasitic and does not contribute to the generated photocurrent. In this work, the absorptivity was calculated from 0.3 to 1.2 μm with a step of 5 nm. We assumed that the internal quantum efficiency (IQE) of the cell was 1. Therefore, all the electron-hole pairs, generated by each

photon absorbed in the c-Si layer, contribute to the photocurrent. Using the absorption in the c-Si layer, we calculated the absorbed current density as

$$J_{sc}(\lambda) = A_{c-Si}(\lambda) * J_{solar}(\lambda) \tag{S1}$$

where $J_{solar}(\lambda)$ is the equivalent Spectral Current Density (SCD) for the AM1.5G spectrum [9] and is calculated as,

$$J_{solar}(\lambda) = P_{solar} \frac{e^{-} \cdot \lambda}{h \cdot c} \tag{S2}$$

P_{solar} is the equivalent spectral power density for the AM1.5G reference spectrum, e^{-} is the electron charge, h is Planck's constant and c is the speed of light in vacuum.

2.2 ALBEDO CONTRIBUTION

Bifacial solar cells can capture light energy from the sun on both sides; the front side absorbs direct sunlight, and the rear one the albedo. The albedo is defined as the measure of the diffuse reflection of solar radiation out of the total solar radiation. We calculate the average absorption spectra ($\overline{A_{c-Si}(\lambda,\theta)}$) on the rear side from Lambert's cosine law, where each absorption spectrum is weighted by the incidence angle. So, albedo's photocurrent on a textured sample models from albedo spectra data of surface materials [10,11] and its expression is given by equation (S3).

$$\begin{aligned} J_{albedo}(\lambda) &= J_{solar}(\lambda) \cdot K_d(\lambda) \cdot \overline{A_{c-Si}(\lambda,\theta)} \\ &= J_{solar}(\lambda) \cdot K_d(\lambda) \cdot \int_0^{\pi/2} \int_0^{\infty} A_{c-Si}(\lambda,\theta) \cdot cos\theta \, d\lambda d\theta \end{aligned} \tag{S3}$$

where $K_d(\lambda)$ is the diffuse reflection function of the surface, and θ is the incidence angle of the albedo. Here, we consider three materials: green grass, concrete, and white sand. The angle sweep was from 0° to 70°, with a step of 10° to obtain the generated photocurrent, the average absorption spectrum is multiplied by the Albedo spectrum of each ground material [10] and the solar irradiance.

2.3 EVALUATION OF THE BIFACIAL SOLAR CELL NET RADIATIVE POWER

In order to determine the thermal performance of the PERC bifacial solar cell proposed, we evaluate the radiative power balance from visible to MIR ranges, given by

$$P_{net} = P_r - P_a - P_{sun} - P_{nr} \tag{S4}$$

where P_r is the radiated power of the cell, P_{sun} and P_a are the absorbed irradiance on the cell from the sun and the atmosphere, respectively, and P_{nr} is the absorbed non-radiative power density from the surrounding. The terms presented in equation (S4) are expressed as

$$P_r = 2\pi \int_0^{\pi/2} sin\theta cos\theta d\theta \int_0^{\infty} B(T_r,\lambda)\varepsilon_r(\lambda,\theta)d\lambda \tag{S5}$$

$$P_{sun} = 2\pi \int_0^{\infty} \varepsilon_r(\lambda, \theta_{sun}) B_{solar}(\lambda) d\lambda \quad \text{(S6)}$$

$$P_a = 2\pi \int_0^{\pi/2} sin\theta cos\theta d\theta \int_0^{\infty} B(T_a, \lambda) \varepsilon_a(\lambda, \theta) \varepsilon_r(\lambda, \theta) d\lambda \quad \text{(S7)}$$

$$P_{nr} = h_c(T_a - T_r) \quad \text{(S8)}$$

In the equations, T_r is the temperature of the radiator and T_a es the ambient temperature, and the term $B(T,\lambda)$ corresponds to the black body radiation according to Plank's law at any temperature and is calculated from

$$B(T, \lambda) = \frac{2hc^2}{\lambda^5} \frac{1}{e^{hc/\lambda kT} - 1} \quad \text{(S9)}$$

h, c, k_B, and λ are the Plank constant, the speed of light in vacuum, the Boltzmann constant, and wavelength, respectively. $\varepsilon_r(\theta,\lambda)$ and $\varepsilon_a(\theta,\lambda)$ are the spectral and directional emissivity/absorptivity of the radiator and atmosphere, respectively. Note that emissivity can be defined by absorptivity according to Kirchhoff's law. The directional emissivity of the atmosphere $\varepsilon_a(\lambda, \theta)$ is calculated as $\varepsilon_a(\lambda, \theta) = 1 - t(\lambda)^{1/cos\theta}$ where $t(\lambda)$ is the atmospheric transmittance in the zenith direction. The atmospheric transmittance depends on the column water vapor and air mass value. In this work, we consider the data from Gemini Observatory, where the column water vapor and air mass are assumed to be 10.0 mm and 1.5, respectively[12]. Finally, B_{solar} is the incident solar irradiation and θ_{sun} the zenith angle between the sun and the vertical of the radiator. Solar irradiance employed was obtained by SMARTS (Simple Model of the Atmospheric Radiative Transfer of Sunshine) code at mid-latitude conditions [13]. In equation (S8), the non-radiative absorption is expressed by non-radiative heat transfer coefficient h_c. This term includes conduction and convection being heavily affected by the weather conditions at each time, the radiator thermal insulation and wind speed.

3. COMPARATIVE PERFORMANCE OF DIFFERENT TEXTURING STRUCTURES IN THE PERC BIFACIAL SOLAR CELL ANALYZED.

The objective of this study was to investigate the potential of integrating texturing techniques to achieve dual benefits in a bifacial PERC solar cell, specifically enhanced light trapping and radiative cooling. Initially, we explored various texturing structures in order to accomplish this objective, ultimately selecting pyramids and inverted pyramids to texture the glass (for radiative cooling) and silicon (for light trapping).

In order to justify the texturing on silicon selected in the paper (inverted pyramids), the net cooling power for the designed bifacial PERC solar cell is calculated with different structures: pyramids, cylinders, and inverted pyramids. For all cases, the calculations were performed on close-packed structures with a pitch and height of 2 and 1.41 μm, respectively.

Fig. S5 shows silicon absorptivity spectra of the previously indicated structures from 0.3 to 5 μm. In order to compare the results, generated current and absorbed solar power will be evaluated. Within the visible range, the selected structure (inverted pyramids) yields the best outcome,

although pyramids exhibit a similar value (58.8 mA/cm^2 vs 58.49 mA/cm^2). However, when the silicon layer of BSC textures with cylinders, the generated photocurrent is 55 mA/cm^2, a 6.3 % lower current generated than the other ones. On the other hand, in terms of the absorbed solar thermal power, the performance of pyramids is even worse than the inverted pyramids from 1.2 μm, with an absorption rate up to 6.8 % higher (118.4 W compared to 112.2 W). The Absorptivity presented by cylinder texturing falls slightly below that achieved with inverted pyramids from 1.2 μm (103.6 W vs 112.2 W), but this reduction is not enough to significantly compensate an extra thermal absorption of 179 W due to the texturing process in the BSC. A summarize of the solar power balance of the analyzed structures is shown in Table S1.

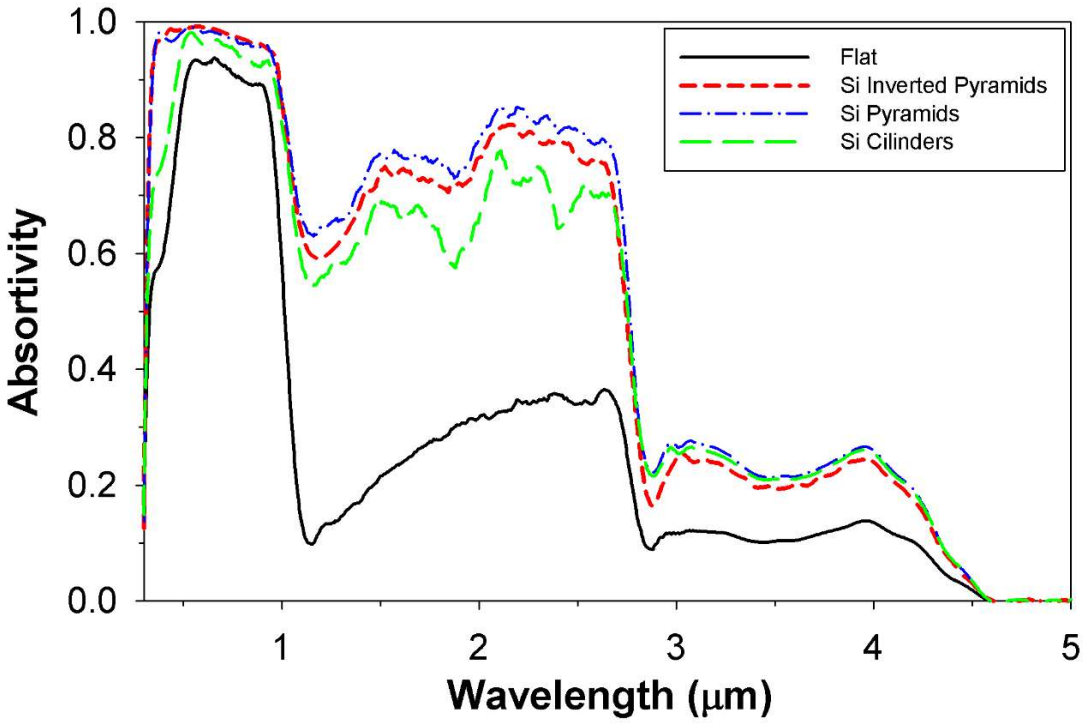

Fig. S5. Dependence of the silicon absorptivity on the BSC textures. (solid black line) flat BSC without textures, (dashed-red line) inverted pyramids textured silicon BSC with structured glass, (dot-dashed blue line) pyramids textured silicon BSC with structured glass, (long-dashed green line) cylinder structured silicon BSC with structured glass.

Structure	*Power reflected (R)*	*Power transmitted (T)*	*Power absorbed in current (P_{ph})*	*Thermal Power Absorbed (P_{th})*
Flat	125.4	141.7	179.3 W	553 W
Inverted Pyramids	50.6 W	4.2 W	212.2 W	732 W
Pyramids	45.5 W	3.4 W	211 W	740 W
Cylinders	72.6 W	12.7 W	197.6 W	717 W

Table S1. Summary of thermal performance for the structured BSC studied.

4. NET POWER BALANCE OF THE PERC BSC's

Next, we present net power calculations for the BSC's presented in the manuscript. Here, the following assumptions have been made for the presented calculation: we assume that the

radiator temperature Tr and ambient temperature Ta, are equal with a value of 25°C (298 K). Second, we calculate the net cooling power of the textured panels during the daytime with absorbed non-radiative power density equal to zero. The spectral transmittance of the atmosphere and the AM1.5 solar radiance employed in the calculations were indicated in the subsection 2.3. The power densities are calculated from 0.3 to 25 μm. The power balance of BSC's analyzed in the paper are presented in Fig. S6. The numerical data are also listed in Table S2. Note that the positive power values represent lost power, while negative power values represent absorbed power.

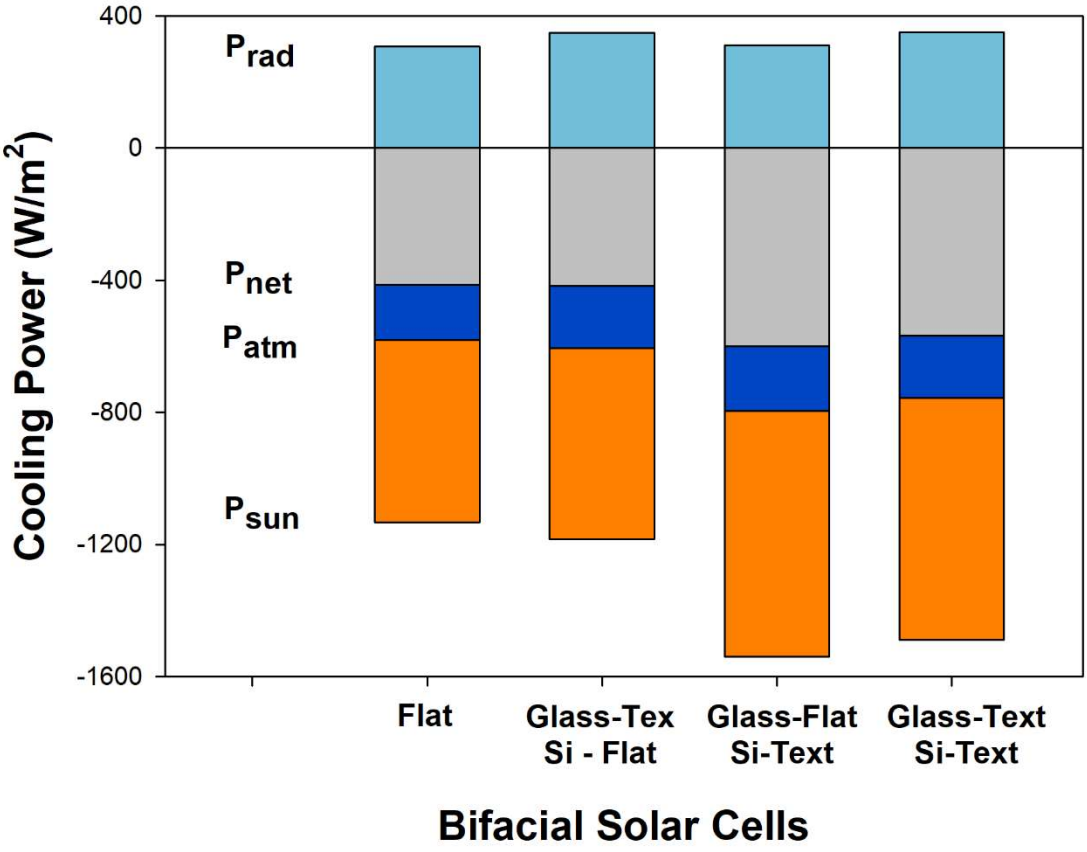

Fig. S6. Distribution of net cooling power (grey), radiated (lightSkyBlue) and atmosphere thermal radiation absorbed (dark blue) and solar (orange) power for each structure presented when ambient and radiator temperatures are equal.

Sample\Term of power	P_{rad} (W)	P_{atm} (W)	P_{sun} (W)	P_{net} (W)
(a) Flat BSC	307.85 W	-167.82 W	-553 W	-412.97 W
(b) Glass Textured flat-silicon BSC	349.53 W	-189.65 W	-577 W	-417.12 W
(c) Flat-glass textured-silicon BSC	310.32 W	-194.53 W	-745 W	-601.07 W
(d) Totally-textured BSC	351.27 W	-187.48 W	-732 W	-568.95 W

Table S2. Summary of thermal performance of BSC studied

References

1. M. Rubin, "Optical properties of soda lime silica glasses," Sol. Energy Mater. **12**, 275–288 (1985).

2. M. A. Green, "Self-consistent optical parameters of intrinsic silicon at 300 K including temperature coefficients," Sol. Energy Mater. Sol. Cells **92**, 1305–1310 (2008).

3. C. D. Salzberg and J. J. Villa, "Infrared Refractive Indexes of Silicon Germanium and Modified Selenium Glass*," J. Opt. Soc. Am. **47**, 244 (1957).

4. P. A. Schumann, W. A. Keenan, A. H. Tong, H. H. Gegenwarth, and C. P. Schneider, "Silicon Optical Constants in the Infrared," J. Electrochem. Soc. **118**, 145 (1971).

5. A. Riverola, A. Mellor, D. Alonso Alvarez, L. Ferre Llin, I. Guarracino, C. N. Markides, D. J. Paul, D. Chemisana, and N. Ekins-Daukes, "Mid-infrared emissivity of crystalline silicon solar cells," Sol. Energy Mater. Sol. Cells **174**, 607–615 (2018).

6. R. Santbergen and R. J. C. van Zolingen, "The absorption factor of crystalline silicon PV cells: A numerical and experimental study," Sol. Energy Mater. Sol. Cells **92**, 432–444 (2008).

7. T. Hirata, K. Akiyama, and T. Morimoto, "Synthesis of b -Si 3 N 4 particles from a -Si 3 N 4 particles," Mater. Lett. **20**, 1191–1195 (2000).

8. J. Kischkat, S. Peters, B. Gruska, M. Semtsiv, M. Chashnikova, M. Klinkmüller, O. Fedosenko, S. MacHulik, A. Aleksandrova, G. Monastyrskyi, Y. Flores, and W. T. Masselink, "Mid-infrared optical properties of thin films of aluminum oxide, titanium dioxide, silicon dioxide, aluminum nitride, and silicon nitride," Appl. Opt. **51**, 6789–6798 (2012).

9. "Reference Air Mass 1.5 Spectra," https://www.nrel.gov/grid/solar-resource/spectra-am1.5.html.

10. M. P. Brennan, A. L. Abramase, R. W. Andrews, and J. M. Pearce, "Effects of spectral albedo on solar photovoltaic devices," Sol. Energy Mater. Sol. Cells **124**, 111–116 (2014).

11. R. Guerrero-Lemus, R. Vega, T. Kim, A. Kimm, and L. E. Shephard, "Bifacial solar photovoltaics - A technology review," Renew. Sustain. Energy Rev. **60**, 1533–1549 (2016).

12. Gemini Observatory, "IR Transmission Spectra," http://www.gemini.edu/?q=node/10789 (accessed October 29, 2020).

13. N. R. E. Laboratory, "Spectral Solar Irradiance, SMARTS: Simple Model of the Atmospheric Radiative Transfer of Sunshine.," https://www.nrel.gov/grid/solar-resource/smarts.html (accessed October 29, 2020).